Effect of the prosthetic mitral valve on vortex dynamics and turbulence of the left ventricular flow

G. Querzoli,[1,a)] S. Fortini,[2] and A. Cenedese[2]
[1]*Dipartimento di Ingegneria del Territorio, Università Degli Studi di Cagliari, Via Marengo 3, Cagliari 09123, Italy*
[2]*Dipartimento di Idraulica Trasporti e Strade, Sapienza Università di Roma, Via Eudossiana 18, Roma 00184, Italy*

(Received 15 May 2009; accepted 6 February 2010; published online 12 April 2010)

Mechanical heart valves implanted in mitral position have a great effect on the ventricular flow. Changes include alteration of the dynamics of the vortical structures generated during the diastole and the onset of turbulence, possibly affecting the efficiency of the heart pump or causing blood cell damage. Modifications to the hemodynamics in the left ventricle, when the inflow through the mitral orifice is altered, were investigated *in vitro* using a silicone rubber, flexible ventricle model. Velocity fields were measured in space and time by means of an image analysis technique: feature tracking. Three series of experiments were performed: one with a top hat inflow velocity profile (schematically resembling physiological conditions), and two with mechanical prosthetic valves of different design, mounted in mitral position—one monoleaflet and the other bileaflet. In each series of runs, two different cardiac outputs have been examined by changing the stroke volume. The flow was investigated in terms of phase averaged velocity field and second order moments of turbulent fluctuations. Results show that the modifications in the transmitral flow change deeply the interaction between the coherent structures generated during the first phase of the diastole and the incoming jet during the second diastolic phase. Top hat inflow gives the coherent structures which are optimal, among the compared cases, for the systolic function. The flow generated by the bileaflet valve preserves most of the beneficial features of the top hat inflow, whereas the monoleaflet valve generates a strong jet which discourages the permanence of large coherent structures at the end of the diastole. Moreover, the average shear rate magnitudes induced by the smoother flow pattern of the case of top hat inflow are nearly halved in comparison with the values measured with the mechanical valves. Finally, analysis of the turbulence statistics shows that the monoleaflet valves yield higher turbulence intensity in comparison with the bileaflet and, with top hat inflow, there is not a complete transition to turbulence. © *2010 American Institute of Physics*.
[doi:10.1063/1.3371720]

I. INTRODUCTION

Fluid dynamics of the left-ventricular flow depends on various factors, such as the ventricle geometry and the cardiac muscle functionality. However the configuration of the mitral valve plays a fundamental role in determining the flow characteristics. It is well known that the replacement of the mitral valve with a prosthesis causes major flow changes which, in turn, affect the functionality of the heart as a pump and possibly cause undesired side effects such as platelet activation, thrombogenesis, and hemolysis.[1–4]

Despite continuous technological development, the study of the ventricular flow *in vivo* is limited by the time and space resolution of the available noninvasive measuring methods, namely, Doppler echocardiography[5,6] and magnetic resonance imaging.[7–9] Details of the fluid mechanics can be appreciated only *in vitro*, where high-resolution techniques can be used. A number of studies has been carried out during the last few decades using laboratory models, initially focusing only on pressure measurements in order to investigate the valve impedance.[10–14] Garitey *et al.*[15] employed a laboratory model of the left ventricle and Doppler echocardiography to document the dynamics of the vortical structures in the ventricular chamber and compare the effects of three prosthetic valves and their orientation. They found that slight differences in the valve design may produce significant differences in the ventricular flow field. After the development of imaging techniques, such as particle image velocimetry (PIV), the flow pattern inside the left ventricle has been investigated in terms of instantaneous maps of velocity and derived quantities.[16–20] Recently, the introduction of high-speed video cameras provided the time resolved variation of the velocity maps, even if most investigators discussed only snapshots at selected points of the cycle rather than time evolutions: Vlachos *et al.*[21] investigated the flow generated by both mechanical and biological prostheses. Cenedese *et al.*[22] investigated the case of a tilting-disk valve using a Lagrangian velocimetry technique called feature tracking, thus obtaining also the statistics of fluid particles accelerations. Akutsu and Fukuda[23] investigated the effect of bileaflet valves with different orientations. Akutsu and Saito[24] compared four bileaflet valves also giving an insight into turbu-

[a)]Author to whom correspondence should be addressed. Electronic mail: querzoli@unica.it.

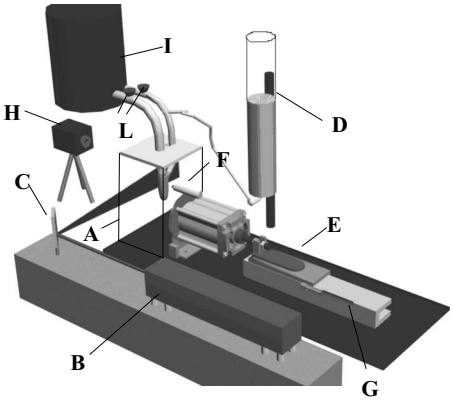

FIG. 1. Experimental model. (A) Ventricle chamber, (B) laser, (C) mirror, (D) compliance, (E) motor, (F) pressure transducer, (G) position transducer, (H) fast camera, (I) tank, and (L) head losses.

lence development in terms of Reynolds stresses. However, these studied computed turbulent fluctuations as deviations from the moving time-average obtained from a single cardiac cycle. Finally, Pierrakos and Vlachos[25] described the ventricular filling within the framework of the vortex ring formation, evaluating the global efficiency of the diastole.

The aim of the present work is to compare the flows generated by three designs of the mitral orifice in order to investigate how it affects the characteristics of the velocity field and, in particular, the onset of turbulence. In the first test condition, a fuse valve was placed far enough upstream to the inlet be completely open, generating a top hat inflow velocity profile, which schematically resembles the main features of the physiological condition, i.e., a single incoming jet, with a nearly uniform velocity profile,[26] not divided by obstacles such as the leaflet of the mechanical prosthesis, with the limitation that native leaflets and cordae tendinae are not reproduced in the model. In the second and third series of experiments, a tilting disk and a bileaflet mechanical valve was placed in mitral position, respectively. The flow is described in terms of phase-averaged maps of quantities describing both properties of the phase-averaged field and of the turbulent fluctuations. The shear strain rate and the turbulence statistics are represented in a form which does not depend on the orientation of the reference frame on the measuring plane.[27] Finally, the time evolution of integral quantities, obtained from the time-resolved velocity measurements, is used to globally describe the shear strain rate and turbulence in the different test conditions.

II. MATERIALS AND METHODS

The ventricular flow was simulated by means of the laboratory model shown in Fig. 1. The model left-ventricle was a conical sack made of silicone rubber in order to be both flexible and transparent. The sack was secured on a circular plate, 56 mm in diameter, connected by means of two Plexiglas conduits to a constant head reservoir. Along the outlet (aortic) conduit a check valve was mounted, whereas the valve placed on the inlet (mitralic) conduit, was changed during the experiments. In the first series of runs, the inlet was set up to obtain a nearly uniform velocity profile at the mitral orifice. To this aim, the function of the mitral valve was performed by a check valve, placed upstream, along the inlet conduit. Preliminary measurements confirmed that the velocity profile at the inlet was approximately uniform. During the other series of runs the check valve was removed and monoleaflet or bileaflet prosthetic valves were placed at the mitral orifice, namely, a Bjork–Shiley monostrut and a bicarbon, both 31 mm in nominal diameter. In the surgical practice, the orientation of the prosthetic valves is chosen by the surgeon on the basis of considerations dependent on fluid dynamics, but also depending on patient specific elements, such as the kind of operation, or the size and shape of the ventricle of the patient (e.g., in order to avoid leaflet impingement by the ventricular wall). In the present experiments, the valves were oriented anatomically, i.e., with the hinge line orthogonal to the line connecting the aortic and mitral orifice centers. The tilting disk of the Bjork–Shiley monostrut was oriented like the aortic leaflet. Figure 2 shows the two valves and their orientation during the experiments. The impedance of the circulatory system was reproduced globally by two adjustable head losses (**L**) and a compliance chamber (**D**) inserted along the conduits. The compliance chamber was made of a sealed Plexiglas cylinder (85 mm in diameter), partially filled with air, and connected to the aortic conduit by means of a T-joint. A rectangular tank (**A**) with transparent, Plexiglas walls housed the left-ventricular model. The volume of the ventricle was changed by moving the piston, placed on the side of the tank. The piston was driven by a computer-controlled linear motor (**E**). A physiologically shaped law of variation of the ventricular volume was used during the tests. It was

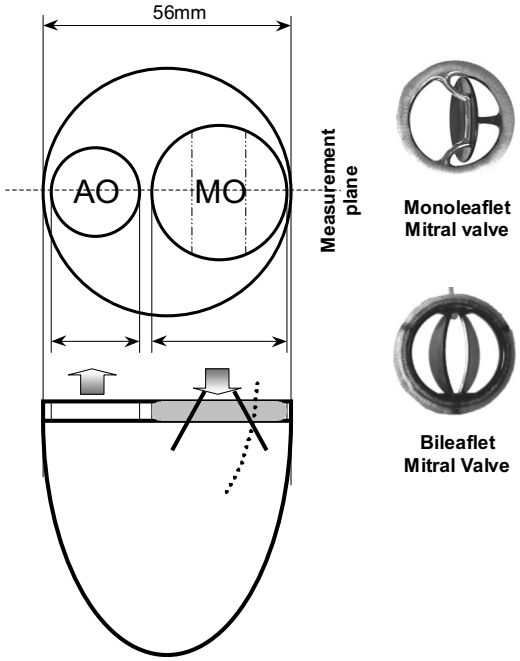

FIG. 2. Orientation of the valve and position of the measurement plane (on the left); pictures of the prosthetic valves used during the experiments (on the right). In the sketch on the left, the leaflets of the bileaflet valve are represented by solid lines and the disk of the monoleaflet valve by a dotted line. The dashed line indicates the measurement plane; the double-dotted dashed lines indicate the hinge axes. AO: aortic orifice. MO: mitral orifice.

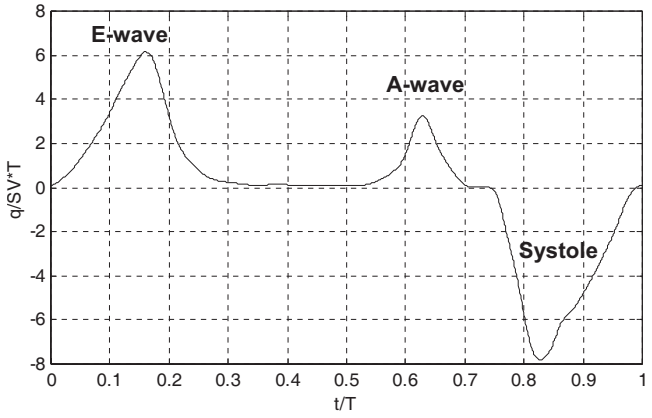

FIG. 3. Nondimensional flow-rate as a function of time.

used also in other numerical and experimental simulations and is derived from clinical data, as reported in Refs. 28 and 29. In Fig. 3, the flow-rate, q, is plotted as a function of time. The flow rate is nondimensionalized by means of the period of the cardiac cycle, T, and the stroke volume, SV. $q(t)$ represents the flow rate through the mitral during the diastole $[0.00T-0.75T]$, and through the aortic valve during the systole $[0.75T-1.00T]$. The diastole is characterized by two peaks separated by an interval, called diastasis, during which the ventricle volume is constant. The first peak, which corresponds to the dilation of the ventricle, is called E-wave. The second peak, called A-wave, is due to the contraction of the atrium. The vertical midplane of the ventricular cavity was illuminated by a 12 W, infrared laser (dashed line in Fig. 2). The working fluid inside the ventricle (distilled water) was seeded with neutrally buoyant particles. The average particle diameter was about 30 μm. A high-speed digital camera (250 frames/s, 480×420 pixel resolution) was triggered by the motor to capture the time evolution of the phenomenon at known instants of the cycle. The acquired images were analyzed to measure the velocity fields on a regular grid (51×51) by means of a feature tracking algorithm. The method, which is described in detail in Ref. 22, is based on the assumption that, for small time intervals, a law of conservation of the light intensity holds true between one frame and the successive. Again, under the assumption of small time intervals, the conservation law is approximated at the first order, and its average on an interrogation window is minimized. The minimization problem results in a set of two linear equations in two unknowns: the two component of the velocity of the fluid in the interrogation windows. In the feature tracking strategy, the interrogation windows are not distributed on a regular grid as in classical PIV algorithms. Rather, they are located in the regions where the set of equations is well conditioned, i.e., where its eigenvalues are high enough. In other words we solve the problem only where a reliable solution can be found. These regions, which are characterized by high light intensity gradients in both spatial directions, are called "good features to track."[30] In fluid velocimetry images, they are typically centered on seeding particles. The spatially unevenly distributed velocity samples are then interpolated on a regular grid.

The resulting spatiotemporal resolution was 1/250 s in time and 1.34 mm in space; high enough to identify the vortical structures generated in the left ventricle and to follow their evolution during the whole cardiac cycle. The geometric scale was 1:1, whereas the duration of the cycle, T, was adjusted in order to keep the Womersley number,

$$\mathrm{Wo} = \sqrt{\frac{D^2}{T\cdot\nu}},$$

and the Reynolds number,

$$\mathrm{Re} = \frac{U\cdot D}{\nu},$$

close to the typical values for a healthy adult (typically, Re ranges from 4000 up to 10 000, and Wo from 20 up to 27).[26,31] In the above definitions, D indicates the maximum diameter of the ventricle, ν the kinematic viscosity, and $U=q_{\max}/A$ ($q_{\max}$ is the maximum flow rate through the mitral valve and A the area of the mitral orifice).

The scale effects on the dynamics of the leaflets can be estimated by the ratio of the fluid dynamic torque to the variation of angular momentum of the leaflets, which is of the order of

$$\frac{\rho U^2 A_l D_M}{\rho_l I\dot{\omega}} \approx \frac{\rho (UT)^2}{\rho_l D_M},$$

where ρ is the fluid density, $A_l \approx {D_M}^2$ is the area of the leaflet of the mechanical valve, D_M indicates the valve diameter, ρ_l is the mass per unit area of the leaflet, $I \approx {D_M}^4$ is the momentum of inertia, and $\dot{\omega}\approx T^{-2}$ is the angular acceleration. Comparing the *in vivo* and *in vitro* values of the quantities in the above ratio, it should be noticed that ρ_l and D_M do not change since the prosthetic valve is the same; though the typical viscosity of the blood is about three times higher than the viscosity of the working fluid (distilled water), their densities are similar (the density of the blood is in the range $1043-1057$ kg m^{-3}).[32] Moreover, provided the stroke volumes used in the present experiments matches the values reproduced *in vivo*, the velocity scale, U, and the period, T, scale reciprocally, and their product remains unvaried. As a consequence, in the present experiments, the ratio of fluid dynamic to inertial torque applied to the leaflets is nearly the same as *in vivo* and scale effects are not expected. However, since the similitude based on the above parameters does not account for the effect of the friction at the hinges and other mechanical characteristics of the prosthetic valves, the following discussion is based on the assumption that these parameters do not affect meaningfully the overall structure of the flow, which is the focus of the of the present investigation. The comparison among present experiments and the structure of the flow presented by other investigators,[21] supports this assumption.

In order to characterize the influence of the variation of stroke volume on the flow structure, for each inflow condition two series of runs were performed, varying the stroke volume from 64 ml to 80 ml. The period, $T=6$ s remained fixed. Each series consisted of 100 runs that were used to compute the phased averages. The turbulence fluctuations

TABLE I. Main parameters describing the experiments.

SV (ml)	T (s)	U (m/s)	Re	W_o
64	6	0.145	8322	22.8
80	6	0.181	10403	22.8

were computed as the deviation from those averages. The main experiment parameters are listed in Table I.

III. RESULTS

A. Average flow

1. Streamlines

Changing the mitral valve influences both the velocity distribution and the initial direction of the fluid entering the ventricle during the diastole. These variations in the inflow affect, in turn, the nature of the coherent structures which are generated during the E-wave and the way in which they interact with fluid entering during the following A-wave.[33] Figure 4 shows the two-dimensional (2D) streamlines (i.e., the streamlines of the two-dimensional measured velocity field) of the phase averaged velocity fields with stroke volume SV=64 ml, and period T=6 s. For each inflow condition, three salient instants of the diastole have been chosen: the end of the E-wave (t/T=0.207), the end of the diastasis (t/T=0.573), and the end of the A-wave, just before the beginning of the systole (t/T=0.707).

In the first row of Fig. 4, the flow generated in absence of any obstacle at the mitral orifice is shown. That configuration is an approximation of the physiological condition and the starting jet entering the ventricle at the beginning of the diastole generates a vortex ring, in accordance with the observations performed *in vivo*.[7,34] The vortex ring is generated during the E-wave, as is clearly shown by the streamlines plotted at t/T=0.207. During its propagation through the ventricle, the part of the vortex ring that is closer to the wall (the right vortex in the plot) tends to move more slowly and to dissipate its energy due to the viscous interaction with the ventricular wall, in accordance with the predictions obtained by means of numerical simulations.[35] At the same time, the opposite part of the vortex can move and increase its size without obstacles. Therefore, at the end of the diastasis, it takes up all the ventricle and its center is in the apical region (center top plot), in general agreement with the observations

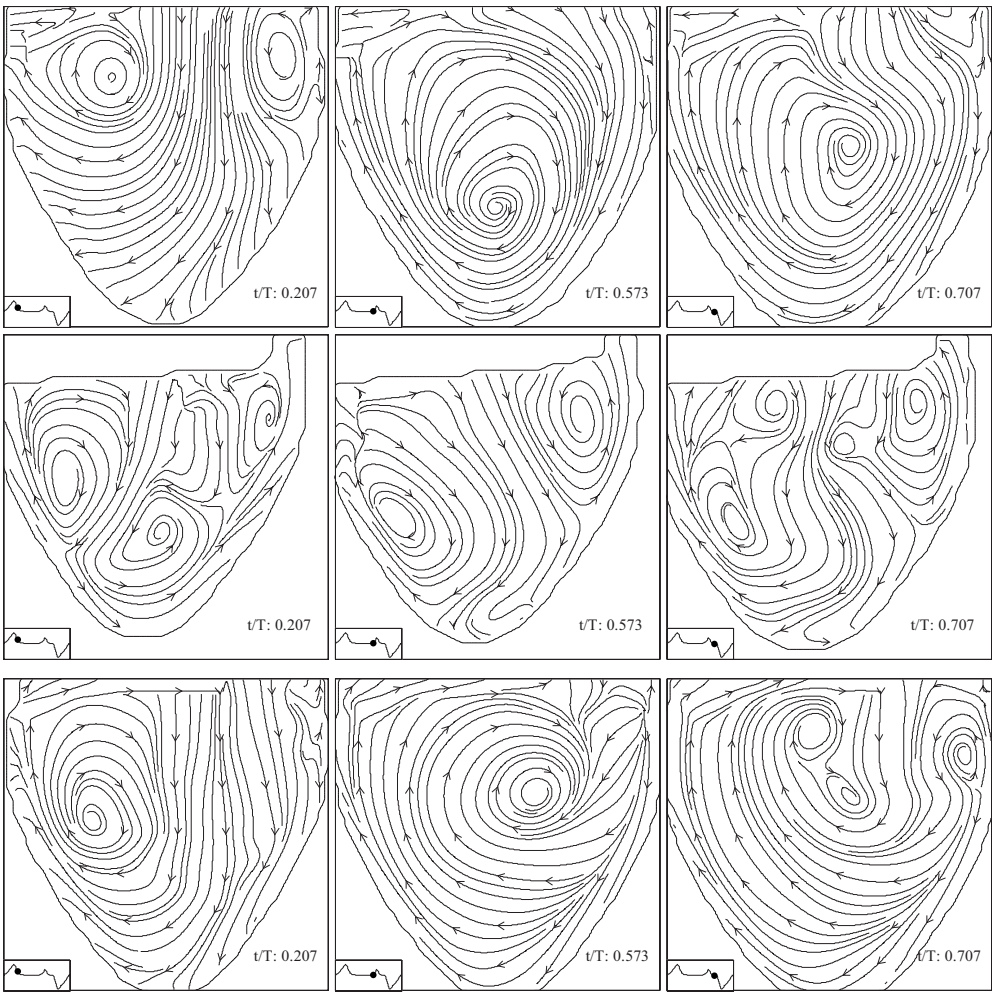

FIG. 4. Streamlines at three instants of the cycle in case of SV=64 ml and period T=6 s. The first row corresponds to uniform inflow, the second to the tilting-disk valve, and the third to the bileaflet valve.

made on healthy subjects by Kim *et al.*[7] using magnetic resonance. The divergence of the streamlines from the center of the vortex is indicative of an out of plane component of the motion. The second diastolic ejection, corresponding to the A-wave, does not break the coherence of the vortex. On the contrary, it tends to increase the vortex strength as the new—lateral—injection of fluid, is deflected toward the posterior ventricular wall (right side of the plot) and contributes to sustain the vortical motion of the fluid (right top plot). At the same time, the center of the vortex moves up and below the mitral (on the right in the plot). The flow pattern at the end of the A-wave seems to be optimal for the successive phase of the cardiac cycle: it is smooth and the fluid in the anterior part of the ventricle (left of the plot) is directed toward the aortic valve. As a matter of fact, the structure of the flow suggests that the energy of the residual motion will not be dispersed but contributes to the expulsion of the fluid during the systole.

The scenario is completely different when a tilting-disk valve is inserted in the mitral position (second row of Fig. 4). During the E-wave, the tilted disk of the valve parts the inflow in two jets: a main jet with a leading vortex ring, directed toward the anterior wall, and a secondary jet on the posterior side of the ventricle. At the end of the E-wave ($t/T=0.207$), three vortices are clearly recognizable on the measurement plane: the two traces of the vortex ring leading the main jet, and only one vortex on the posterior side of the secondary jet. In this case, the main vortex ring has already reached the opposite wall, meaning a higher propagation velocity compared with the case of uniform inflow. During the diastasis the two vortices of the main jet tend to separate, moving along the ventricular walls, whereas the third vortex dissipates because of the interaction with the ventricular wall. At the same time, the vortex on the left side of the plot increases in size. At the end of the diastasis ($t/T=0.573$), the flow is dominated by two vortices: one just below the mitral valve and the other on the opposite wall, closer to the apex. As the inflow reappears, at the A-wave, the main jet is directed straight to the core of the left vortex, breaking its coherence and reducing the residual motion in a collection of small vortices moving around within the ventricle as can be observed looking at the streamlines plotted at $t/T=0.707$. In that case, the energy of the residual motion does not seem to be available to help fluid ejection during the systole; on the contrary, the residual vorticity, as advected through the aortic valve, may contribute to the generation of turbulence.

An intermediate scenario is shown in the plots representing the flow generated by the bileaflet valve (third row of Fig. 4): during the E-wave, the inflow is divided into three jets moving straight downward. On average, they produce a single, wide stream moving downward and a large, clockwise, vortex located below the aortic valve (bottom left plot of Fig. 4). During the diastasis the vortex increases in size and its core moves to the center of the ventricle. Therefore, at the end of the diastasis (bottom center plot), the streamline pattern is similar to the one observed in case of uniform inflow (top center of Fig. 4). Also in that case, the convergence of the vortex streamlines indicates the existence of an out of plane motion. During the atrial contraction, despite some interference between the jet and the vortex core, the fluid entering the ventricle seems to increase the overall rotation of the fluid. As a result, at the end of the A-wave, an overall clockwise rotation dominates the fluid and the streamlines along the anterior ventricular wall are directed toward the aortic valve (bottom right plot of Fig. 4). As in the first case, the flow pattern at that time seems favorable to the successive systole, since most of the energy remaining from the E-wave, and provided to the fluid during the A-wave, can usefully contribute to the fluid ejection.

B. Shear stresses

The streamlines presented above clearly depict the main features of the flow, but do not highlight the intensity of the spatial velocity gradients, which are known to be related to red cell damage (hemolysis) through the viscous shear stresses.[36,37] In general, the shear strain rate is defined relative to a plane and depends on its orientation. At each location, there is an orientation maximizing this shear strain rate. That maximum value is the critical one for the possible blood damaging. The expression used for the evaluation of the maximum shear rate, $e_{\max}$, at a given location is[22,27]

$$e_{\max} = (e_1 - e_2)/2,$$

where e_1 and e_2 indicate, respectively, the maximum and minimum eigenvalues of the deformation velocity tensor. The expression above only takes into account the in-plane velocity components, but the general structure of the flow suggests that the off-plane gradients are presumably much smaller than the in-plane ones; therefore it can be regarded as a reasonably good approximation of the 3D maximum shear rate.[38]

The measurements herein yield the spatiotemporal evolution of $e_{\max}$. However, in order to reduce that huge amount of data, the spatial structure is presented at the instant when the shear rate attains its maximum for the three inlet conditions, while the time evolution in the different conditions is discussed in terms of the average value of $e_{\max}$ over the whole ventricle.

In Fig. 5, the maximum shear rate, $e_{\max}$, nondimensionalized by the inverse of the advective time $T_a=D/U$, is drawn in the same test conditions as in Fig. 4. It is related to the nondimensional shear stress by the inverse of the Reynolds number:

$$\frac{\tau_{\max}}{\rho U^2} = \frac{2}{\mathrm{Re}}(e_{\max} T_a).$$

The maps are drawn at the end of the E-wave ($t/T=0.207$), i.e., around the time of the cycle when the spatially averaged shear rate is observed to reach the highest values whatever the mitral valve (see Fig. 6 and the related discussion in the following of the section). The uniform inflow generates a smooth velocity field in the ventricle, characterized by a wide jet trailing a well organized vortex ring (left plot of Fig. 5). That flow structure causes low velocity gradients and the level of shear rate is low almost everywhere. Maximum values are located at the jet front and at the borders of the vortices. The scenario is completely different with the tilting-

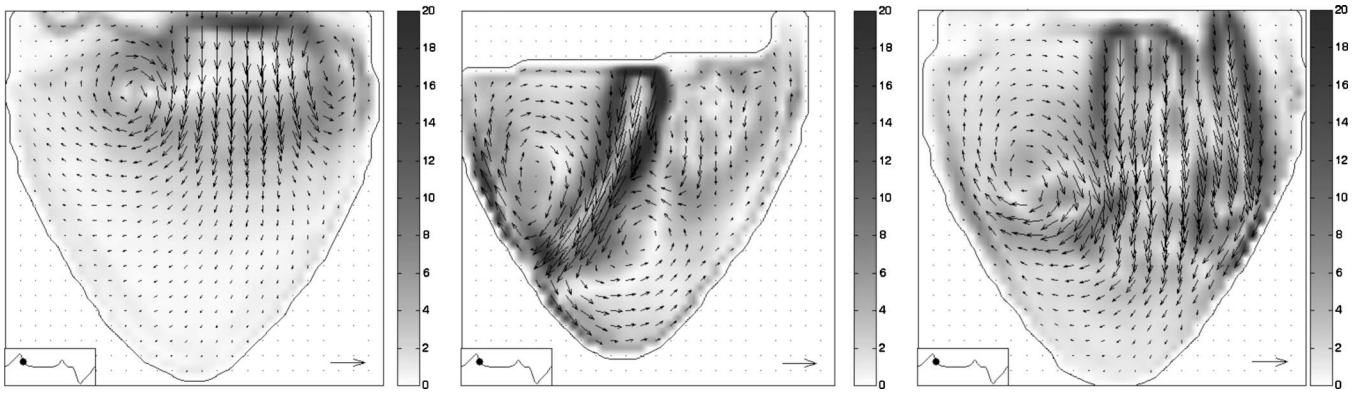

FIG. 5. Average velocity field (vectors) and nondimensional maximum shear rate (gray scale) at $t/T=0.207$ ($T=6$ s and SV=64 ml). Uniform inflow on the left, tilting-disk valve in center, and bileaflet valve on the right. The horizontal vector on the lower right corner of the plots indicates the velocity scale U. The dot on the flow-rate plot on the lower left corner indicates the considered point of the cycle.

disk valve (center plot of Fig. 5): the flow deflected by the disk generates a narrow and intense jet which dominates the flow. This is the case which leads to the maximum local values of the shear rate. Highest values are located at the border of the jet, close to the valve, and at the opposite ventricular wall, where the impacting jet is deflected along the walls. The bileaflet valve generates a multijet flow, giving the maximum values of the shear rate which are intermediate in comparison with the previous cases (right plot of Fig. 5). However, the region occupied by meaningful values is larger. There is an apparent effect of the impact of the incoming flow on the wall (right of the plot), generating the highest shear rates of the field, and a region of relatively high shear is at the border of the rightmost jet.

The time evolution of the average, nondimensional shear rate $\langle e_{\max}\rangle \cdot T_a$ is shown in Fig. 6 for the different test conditions, where angle brackets indicate the phase average over the measuring area within the ventricle. The six curves have three relative maxima at more or less the same times, regardless of both the inlet valve and the stroke volume. The first peak is the highest and corresponds to the end of the E-wave, i.e., the situation described in the maps of Fig. 5. The second peak is due to the A-wave, whereas the third is related to the converging flow through the aortic valve, during the systole. Noisy fluctuations at the beginning of the E-wave and during the initial part of the systole are the consequence of the reflections and shadows generated at the opening and closing of the leaflets of the mitral valve. The main variations in magnitude occur at the first peak. The nondimensional values do not depend greatly on the stroke volume, confirming the validity of the chosen scaling. The peak values generated by the two mechanical valves are quite similar. This is due to the fact that the bileaflet valve generates a wide area of relatively high values whereas the tilting-disk valve generates a narrower area of higher values, leading nearly to the same average value. The smooth flow generated by the open mitral orifice causes significantly lower values compared to the mechanical valves: the main peak is about one-half of the other

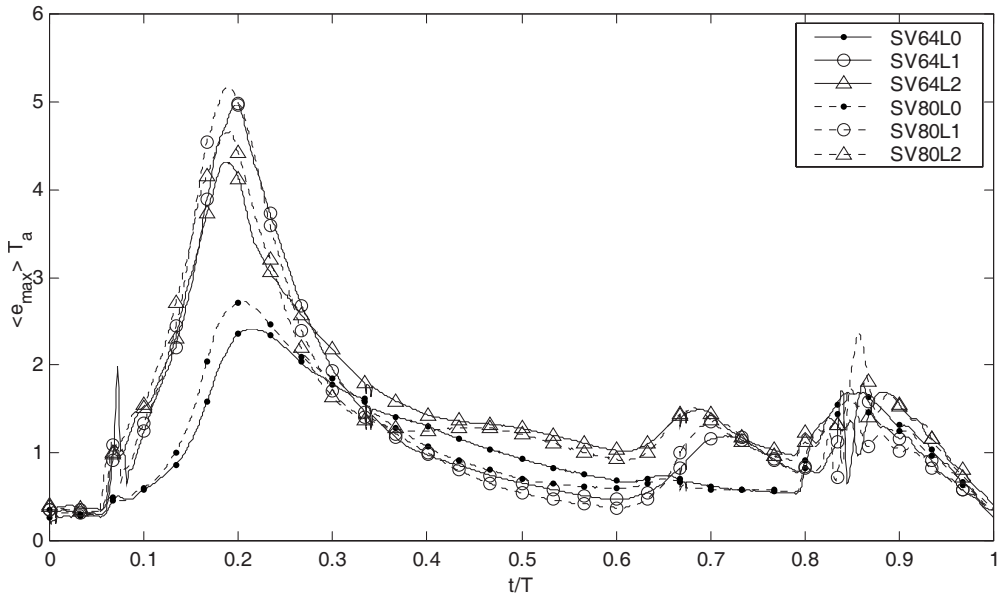

FIG. 6. Average nondimensional shear rate during the cardiac cycle. In the legend, the two digits after SV indicate the stroke volume in milliliters, while L0, L1, and L2 refer to the uniform inflow, tilting-disk valve, and bileaflet valve, respectively.

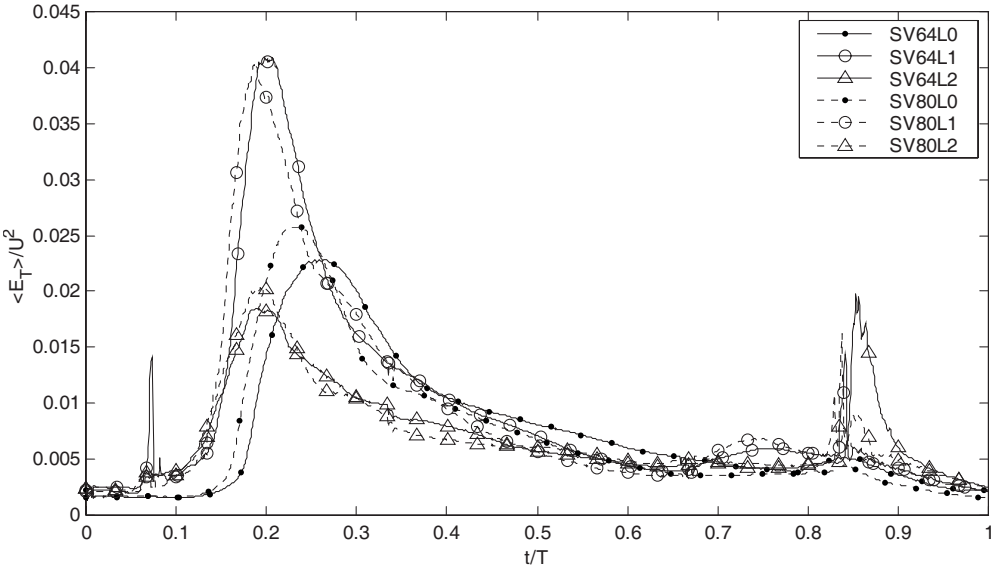

FIG. 7. Average, nondimensional turbulence kinetic energy as a function of time. In the legend, the two digits after SV indicate the stroke volume in milliliters, while L0, L1, and L2 refer to the uniform inflow, tilting-disk valve, and bileaflet valve, respectively.

cases, the second peak (generated by the second injection during the A-wave) is nearly absent, whereas the last peak, corresponding to the systole, is similar to the other cases since it is not related to the inflow.

It is known that hemolysis and platelet activation are also related to an effect of damage accumulation.[4] Since the magnitude of the average shear rate depends also on the width of the region characterized by high values, it is indicative of the number of blood cells involved in high shear stresses levels. Therefore, $\langle e_{\max} \rangle$ can be regarded as related to the potential damage of the accumulation effect. From this point of view, it should be noted that the tilting disk valve mitigates the high shear rate magnitude with a relatively small area of high-level shear rate, i.e., with spatially concentrated shear.

C. Turbulence

During the cardiac cycle, the ventricular flow is characterized by a strong variability in time, with the instantaneous Reynolds number ranging from vanishingly small values to values high enough for the flow to become unstable and possibly turbulent during the diastolic phase. In order to investigate the occurrence of turbulence, the second order statistics of the velocity fluctuations have been analyzed. We made 2D in-plane measurements, therefore only the 2D Reynolds tensor was considered. In particular, we chose the turbulent kinetic energy,

$$E_T = \overline{u'^2} + \overline{v'^2},$$

to describe the normal Reynolds stresses, and the maximum Reynolds shear stress for the turbulent shear stresses, which is defined similarly to the shear rate as

$$\tau_{R\,\max} = (\tau_{R1} - \tau_{R2})/2,$$

where τ_{R1} and τ_{R2} indicate the maximum and minimum eigenvalues of the Reynolds tensor, respectively. As a consequence, both quantities discussed hereafter are frame independent. Though symmetry arguments suggest that the maximum Reynolds shear rate is a good approximation of the real one,[38] the absence of the third velocity component may affect the computation of the turbulent kinetic energy. However, the data presented here give insight into the onset of instability and the intensity of turbulence.

1. Turbulent kinetic energy

In Fig. 7, the nondimensional turbulent kinetic energy phase-averaged over the measurement region, $\langle E_T \rangle / U^2$, is plotted as a function of the nondimensional time. The curves corresponding to the same inlet conditions are in good agreement, confirming the validity of the scaling. Disregarding the sharp, noisy peaks at $t/T \cong 0.07$ and $t/T = 0.85$, due to the light reflections generated by the movements of the leaflets at the opening and closing of the prosthetic valve, the six plots exhibit a main peak corresponding to the E-wave. The strong jet due to the deflection of the flow by the tilted disk generates a peak value which is more or less twice than with the bileaflet valve or uniform inflow. In contrast with the above-mentioned average shear rate, the peak values depend on which mitral valve is mounted. With mechanical valves the peak is reached at $t/T = 0.19$ and $t/T = 0.20$ (bileaflet and tilting disk, respectively), whereas with uniform inflow the onset of turbulence is delayed and the peak is reached at $t/T = 0.25$. There is a meaningful local increase corresponding to the A-wave only with the tilting-disk valve, due to the breaking of the vortex generated during the E-wave.

The spatial distribution of the nondimensional turbulent kinetic energy can be observed in Fig. 8, where the maps are drawn for the three inlet conditions $T = 6$ s, and SV = 64 ml. The fields are plotted at the time when $\langle E_T \rangle / U^2$ is a maximum. In the case of uniform inflow there is a zone of relatively high turbulence in the jet trailing the vortex ring, which becomes unstable as the flow through the mitral de-

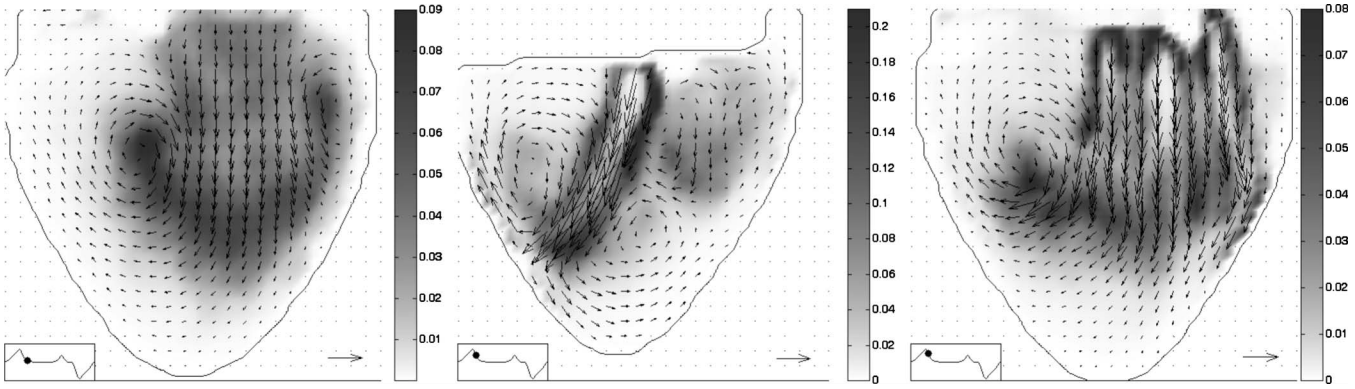

FIG. 8. Velocity field (vectors) and average nondimensional turbulent kinetic energy. Left plot: uniform inflow, $t/T=0.25$. Center plot: tilting-disk valve, $t/T=0.20$. Right plot: bileaflet valve, $t/T=0.19$.

celerates. Other high levels are found at the leading border of the jet and in the proximity of the core of the vortex ring, mainly due to small differences in the position of the vortex ring between cycles in regions where the velocity gradients are high.

The scenario is different in the flow generated by mechanical, prosthetic valves and is characterized by one or more jets, and the regions of high turbulence are located mainly at the border of the jets, where the flow becomes unstable due to the shear.

2. Reynolds shear stresses

Reynolds shear stresses are known to be one of the causes of hemolysis related to mechanical prosthetic valve implantation.[39] Highest values are typically found in close proximity to the valve. They depend on the particular valve model and require very detailed investigation of the transvalvular flow, and are out of the scope of the present paper.[17,18,40] However, the damage accumulation effect, leading to cell senesce, is related to both the magnitude and extent of the high Reynolds stress region within the ventricular flow.[4] Therefore, the phase average over the ventricle of the maximum Reynolds shear stress, $\langle \tau_{R\,\max} \rangle$, is a significant indicator of the potential damage caused by the general structure of the ventricular flow.

The time evolution of $\langle \tau_{R\,\max} \rangle$, plotted in Fig. 9, exhibits the same main features as the turbulent kinetic energy: ignoring the noisy peaks corresponding to the opening and closing of the mitral valve, a main peak at the same times as for the turbulent kinetic energy. Moreover, the cases of bileaflet valve and uniform inflow attain about the same maximum magnitude, roughly half that of the tilting-disk valve. The instantaneous maps of $\langle \tau_{R\,\max} \rangle$, plotted in Fig. 10, demonstrate that the high peak of the average Reynolds shear stress is due to the contribution of the turbulent layer at the boundary of the strong jet generated by the tilted disk when the monoleaflet valve is open. With uniform inflow, the highest levels are at the leading front of the jet flow developing through the ventricle and at the core of the vortex ring. Finally, with the bileaflet valve, the high Reynolds shear

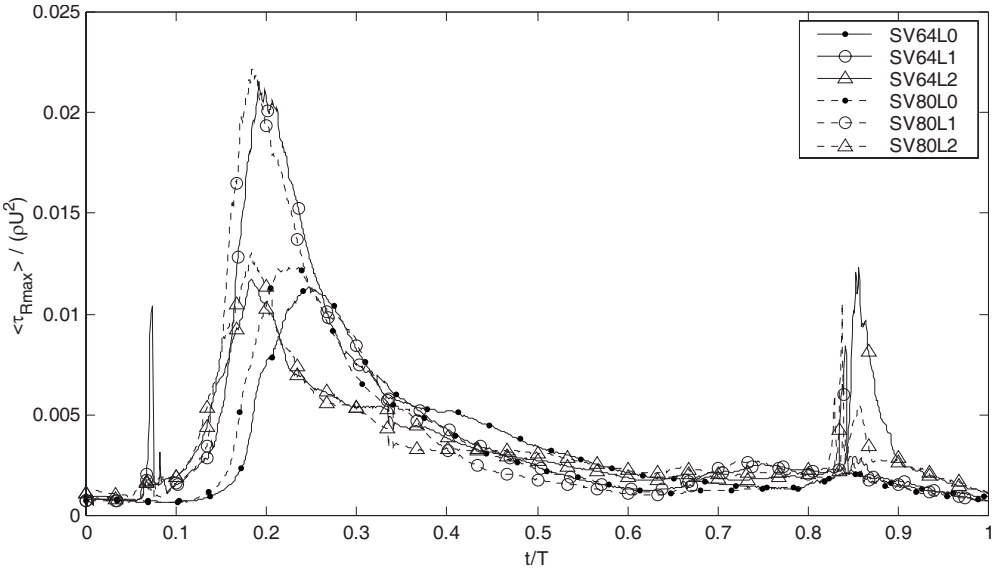

FIG. 9. Nondimensional maximum Reynolds shear stresses phase averaged over the ventricle. In the legend, the two digits after SV indicate the stroke volume in milliliters, while L0, L1, and L2 refer to the uniform inflow, tilting-disk valve, and bileaflet valve, respectively.

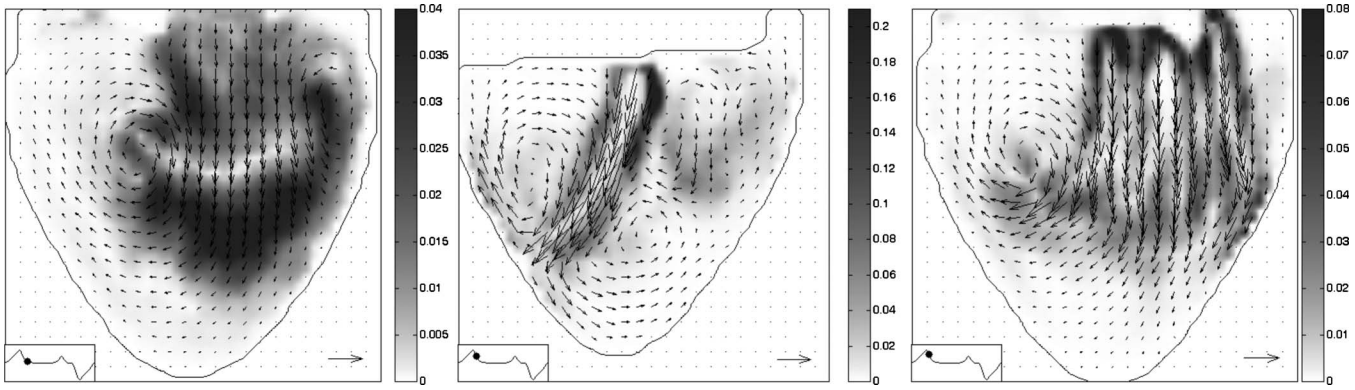

FIG. 10. Velocity field (vectors) and average nondimensional Reynolds shear stresses. Left plot: uniform inflow, $t/T=0.25$. Center plot: tilting-disk valve, $t/T=0.20$. Right plot: bileaflet valve, $t/T=0.19$.

stresses are found in the narrow regions of interaction between the three jets. As a consequence, the scale of the vortices remains small and the magnitude of the Reynolds shear stresses remains low compared to the monoleaflet case.

IV. CONCLUSIONS

The present investigation focused on the comparison of the ventricular flow with mitral inflow generated by mechanical valves of different design. The experiments and measurements were designed to capture the general features of the flow, not the details related to the particular valve model, with the aim of understanding the effects caused by the different overall valve structure. Analysis of the flow patterns indicates that modifications in the transmitral flow affect deeply the interaction between the coherent structures generated during the first filling phase and the inflow corresponding to the atrial contraction at the end of the diastole. Top hat inflow (i.e., similar to the native transmitral flow) creates a flow structure which seems to be superior with respect to the other tested conditions. In fact, the coherence of the large vortex generated during the E-wave is not broken during the successive A-wave. Therefore there is less production of turbulence, and the large vortex, which is still present at the beginning of the diastole, orients the blood velocity toward the aortic valve, aiding the systolic function. The three-jet structure of the flow generated by the bileaflet valve creates a similar coherent vortex which, although lightly perturbed, conserves its beneficial effects on the systole. On the contrary, the strong, oblique jet generated by the tilting-disk valve prevents the flow from organizing into large coherent structures at the end of the diastole.

In terms of shear strain rate, the two mechanical valves are more or less equivalent, whereas the uniform inflow yields to a peak of roughly one-half the phase average values. The localized shear rate measured with the monoleaflet valve is more concentrated than that with the three jets of the bileaflet valve.

The analysis of turbulence provides a different picture: the bileaflet valve and the uniform inflow are nearly identical. The tilting disk design creates more turbulence both in terms of normal and shear stresses. It should be noted that visual inspection of the time evolution of the turbulence suggests that one should pay particular attention to the position of the jets and of the coherent structures generated, in particular, in physiological-like conditions. Slight differences in location at different cycles are related to the initial development of the flow instability rather than real turbulence, even if they yield high fluctuations in the regions where the velocity gradients are high.

ACKNOWLEDGMENTS

The authors are grateful to Dr. Marco Marchetti for valuable help in performing measurements and setting up the experimental facilities, and to Jason Hyatt for carefully reading the draft and providing valuable suggestions.

[1] B. M. Rodgers and D. C. Sabitson, Jr., "Hemolytic anemia following prosthetic valve replacement," Circulation **39**, I155 (1969).
[2] M. J. Garcia, P. Vandervoort, W. J. Stewart, B. W. Lytle, D. M. Cosgrove, J. D. Thomas, and B. P. Griffin, "Mechanisms of hemolysis with mitral prosthetic regurgitation study using transesophageal echocardiography and fluid dynamic simulation," J. Am. Coll. Cardiol. **27**, 399 (1996).
[3] G. Ismeno, A. Renzulli, A. Carozza, M. De Feo, M. Iannuzzi, P. Sante, and M. Cotrufo, "Intravascular hemolysis after mitral and aortic valve replacement with different types of mechanical prostheses," Int. J. Cardiol. **69**, 179 (1999).
[4] Y. Alemu and D. Bluestein, "Flow-induced platelet activation and damage accumulation in a mechanical heart valve: Numerical studies," Artif. Organs **31**, 677 (2007).
[5] Y. Kawano, K. Ohmori, Y. Wada, I. Kondo, K. Mizushige, S. Senda, S. Nozaki, and M. Kohno, "A novel color M-mode Doppler echocardiographic index for left ventricular relaxation: Depth of the maximal velocity point of the left ventricular inflow in early diastole," Heart Vessels **15**, 205 (2000).
[6] R. Verdonck, K. Dumont, P. Segers, S. Vandenbogaerde, and G. van Nooten, "Mock loop testing of On-X prosthetic mitral valve with Doppler echocardiography," Artif. Organs **26**, 872 (2002).
[7] W. Y. Kim, P. G. Walker, E. M. Pederson, J. K. Poulsen, S. Oyre, K. Houlind, and A. P. Yoganathan, "Left ventricular blood flow patterns in normal subjects: A quantitative analysis by three-dimensional magnetic resonance velocity mapping," J. Am. Coll. Cardiol. **26**, 224 (1995).
[8] H. Machlera, M. Perthelb, G. Reiterc, U. Reiterc, M. Zinkd, P. Bergmanna, A. Waltensdorferd, and J. Laa, "Influence of bileaflet prosthetic mitral valve orientation on left ventricular flow—an experimental in vivo magnetic resonance imaging study," Eur. J. Cardiothorac Surg. **26**, 747 (2004).
[9] R. Merrifield, Q. Long, X. Y. Xu, P. J. Kilner, D. N. Firmin, and G. Z. Yang, "Combined CFD/MRI analysis of left ventricular flows," in *Medical Imaging and Augmented Reality*, edited by G.-Z. Yang and T. Jiang (Springer-Verlag, Berlin, 2004), p. 229.

[10]B. J. Bellhouse, "Fluid mechanics of a model valve and left ventricle," Cardiovasc. Res. **6**, 199 (1972).
[11]H. Reul, N. Talukder, and E. W. Müller, "Fluid mechanics of the natural mitral valve," J. Biomech. **14**, 361 (1981).
[12]J. Kohler, G. Ehrentraut, and B. Stormer, "Haemodynamics of four new prosthetic heart values," in Proceedings of European Society of Artificial Organs VIII, Copenhagen (1981), p. 361.
[13]L. N. Scotten, D. K. Walker, and R. T. Brownlee, "The Bjork–Shiley and Ionescu–Shiley heart valve prostheses. In vitro comparison of their hydrodynamic performance in the mitral position," Scand. J. Thorac. Cardiovasc. Surg. **17**, 201 (1983).
[14]J. Fisher, G. R. Jack, and D. J. Whetley, "Design of a function test apparatus for prosthetic heart valves. Initial results in the mitral position," Clin. Phys. Physiol. Meas. **7**, 63 (1986).
[15]V. Garitey, T. Gandelheid, J. Fusezi, R. Pelissier, and R. Rieu, "Ventricular flow dynamic past bileaflet prosthetic heart valves," Int. J. Artif. Organs **18**, 380 (1995).
[16]D. Bluestein, E. Rambod, and M. Gharib, "Vortex shedding as a mechanism for free emboli formation in mechanical heart valves," J. Biomech. Eng. **122**, 125 (2000).
[17]V. Kini, C. Bachmann, A. Fontaine, S. Deutsh, and J. M. Tarbell, "Integrating particle image velocimetry and laser Doppler velocimetry measurements of the regurgitant flow field past mechanical heart valves," Artif. Organs **25**, 136 (2001).
[18]Ch. Brücker, U. Steinseifer, W. Schrode, and H. Reul, "Unsteady flow through a new mechanical heart valve prosthesis analysed by digital particle image velocimetry," Meas. Sci. Technol. **13**, 1043 (2002).
[19]J. Cooke, J. Hertzberg, M. Boardman, and R. Shandas, "Characterizing vortex ring behaviour during ventricular filling with Doppler echocardiography: An in vitro study," Ann. Biomed. Eng. **32**, 245 (2004).
[20]F. Mouret, L. Kadem, E. Bertrand, J. D. Dumesnil, P. Pibarot, and R. Rieu, "Mitral prosthesis opening and flow dynamics in a model of left ventricle: An in vitro study on a monoleaflet mechanical valve," Cardiovasc. Eng. **5**, 13 (2005).
[21]O. Pierrakos, P. P. Vlachos, and D. P. Telionis, "Time-resolved DPIV analysis of vortex dynamics in a left ventricular model through bileaflet mechanical and porcine heart valve prostheses," J. Biomech. Eng. **126**, 714 (2004).
[22]A. Cenedese, Z. Del Prete, M. Miozzi, and G. Querzoli, "A laboratory investigation of the flow in the left ventricle of a human heart with prosthetic, tilting-disk valves," Exp. Fluids **39**, 322 (2005).
[23]T. Akutsu and T. Fukuda, "Time-resolved particle image velocimetry and laser Doppler anemometry study of the turbulent flow field of bileaflet mechanical mitral prostheses," J. Artif. Organs **8**, 171 (2005).
[24]T. Akutsu and J. Saito, "Dynamic particle image velocimetry flow analysis of the flow field immediately downstream of bileaflet mechanical mitral prostheses," J. Artif. Organs **9**, 165 (2006).
[25]O. Pierrakos and P. P. Vlachos, "The effect of vortex formation on left ventricular filling and mitral valve efficiency," J. Biomech. Eng. **128**, 527 (2006).
[26]B. O. Haugen, S. Berg, K. M. Brecke, S. O. Samstad, S. A. Slørdahl, T. Skjærpe, and H. Torp, "Velocity profiles in mitral blood flow based on three-dimensional freehand colour flow imaging acquired at high frame rate," Eur. J. Echocardiogr. **1**, 252 (2000).
[27]M. Grigioni, C. Daniele, V. D'Avenio, and V. Barbaro, "Evaluation of the surface-averaged load exerted on a blood element by the Reynolds shear stress field provided by artificial cardiovascular devices," J. Biomech. **35**, 1613 (2002).
[28]B. Baccani, F. Domenichini, G. Pedrizzetti, and G. Tonti, "Fluid dynamics of the left ventricular filling in dilated cardiomiopathy," J. Biomech. **35**, 665 (2002).
[29]F. Domenichini, G. Querzoli, A. Cenedese, and G. Pedrizzetti, "Combined experimental and numerical analysis of the flow structure into the left ventricle," J. Biomech. **40**, 1988 (2007).
[30]J. Shi and C. Tomasi, "Good features to track," in Proceedings of IEEE Conference on Computer Vision and Pattern Recognition (CVPR94), Seattle, 1994.
[31]C. A. Walsh and P. Wilde, *Practical Echocardiography* (Cambridge University Press, New York, 2005), p. 218.
[32]H. G. Hinghofer-Szalkay and J. E. Greenleaf, "Continuous monitoring of blood volume changes in humans," J. Appl. Physiol. **63**, 1003 (1987).
[33]G. Pedrizzetti and F. Domenichini, "Asymmetric opening of a simple bileaflet valve," Phys. Rev. Lett. **98**, 214503 (2007).
[34]H. Bot, J. Verburg, B. J. Delemarre, and J. Strackee, "Determinants of the occurrence of vortex rings in the left ventricle during diastole," J. Biomech. **23**, 607 (1990).
[35]F. Domenichini, G. Pedrizzetti, and B. Baccani, "Three-dimensional filling flow into a model left ventricle," J. Fluid Mech. **539**, 179 (2005).
[36]C. Nevaril, J. Hellums, C. J. Alfrey, and E. Lynch, "Physical effects in red blood cell trauma," AIChE J. **15**, 707 (1969).
[37]P. L. Blackshear, "Mechanical hemolysis in flowing blood," in *Biomechanics: Its Foundations and Objectives*, edited by Y. C. Fung, N. Perrone, and M. Anliker (Prentice-Hall, Englewood Cliffs, NJ, 1972), p. 501.
[38]A. A. Fontaine, J. T. Ellis, T. M. Healy, J. Hopmeyer, and A. P. Yoganathan, "Identification of peak stresses in cardiac prostheses. A comparison of two-dimensional versus three-dimensional principal stresses analyses," ASAIO J. **42**, 154 (1996).
[39]M. Grigioni, C. Daniele, V. D'Avenio, and V. Barbaro, "A discussion on the threshold limit for hemolysis related to Reynolds shear stress," J. Biomech. **32**, 1107 (1999).
[40]Y. Woo and A. P. Yoganathan, "In vitro pulsatile flow velocity and shear stress measurements in the vicinity of mechanical mitral heart valve prostheses," J. Biomech. **19**, 39 (1986).